Solar Energy Materials & Solar Cells 278 (2024) 113156

Contents lists available at ScienceDirect

Solar Energy Materials and Solar Cells

journal homepage: www.elsevier.com/locate/solmat

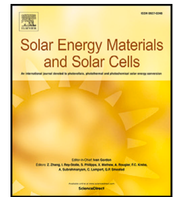

Long-term stability of TOPCon solar cell precursor structures based on Ga-doped Cz-Si

Joshua Kamphues [a,*], Jessica Lison [a], Jana-Isabelle Polzin [b], Andreas Wolf [b], Jan Lossen [c], Axel Herguth [a], Giso Hahn [a], Fabian Geml [a]

[a] University of Konstanz, Department of Physics, Universitätstrasse 10, Konstanz, 78464, Germany
[b] Fraunhofer Institute for Solar Energy Systems, Heidenhofstrasse 2, Freiburg, 79110, Germany
[c] International Solar Energy Research Center Konstanz e. V., Rudolf-Diesel-Strasse 15, Konstanz, 78467, Germany

ARTICLE INFO

Keywords:
Ga-doped silicon
TOPCon
Hydrogen
Excess carrier lifetime
LeTID

ABSTRACT

In this study, the impact of tunnel oxide passivated contact (TOPCon) solar cell precursor structures on commercial Ga-doped Czochralski silicon is investigated regarding bulk- and surface-related degradation. Two sample types, symmetrical poly-Si structures and asymmetrical samples featuring various passivation stacks used in TOPCon cells are examined.

It is found that firing temperatures well above 800 °C lead to blistering and a significant reduction in performance for symmetrical TOPCon structures, reducing iV_{OC} to below 700 mV. Treatment at an elevated temperature under constant illumination revealed that a significant degradation could only be observed at measured firing peak temperatures above 750 °C. While it is found that an AlO_x interlayer underneath a SiN_y:H layer effectively reduces the extent of degradation without an (n)poly-Si layer, it seems to be less effective on top of (n)poly-Si layers.

Another experiment on the long-term stability revealed that surface-related degradation (SRD) is significantly reduced by the usage of symmetrical TOPCon structures and for a sample passivated with an $SiO_z/AlO_x/SiN_y$:H stack. Compared to reference samples processed without TOPCon structures, a notable reduction in the extent of light- and elevated temperature-induced degradation (LeTID) is achieved in the samples featuring TOPCon structures, which is due to less hydrogen in-diffusion from passivation layer stacks into the bulk during the firing process.

1. Introduction

Nowadays, the photovoltaic industry is steadily shifting solar cell production towards cells with TOPCon technology by replacing the passivated emitter and rear cell (PERC) approach due to the potential of the TOPCon cell structure to enable higher cell efficiencies [1,2]. By this shift, an increase in Ag consumption could be the result, which is a limited resource. Despite the massive production shift towards n-type Cz–Si [3], Ga-doped material still offers cost-efficient production and the possibility for highly efficient cell concepts, e.g. pIBC solar cells [4–6]. Process costs could be lowered by the usage of a $POCl_3$ diffusion instead of BCl_3 or BBr_3 as lower temperature and processing times can be used and gettering might be more effective. But regardless of cell architecture, long-term stability remains a challenge for the PV industry.

Literature indicates that B-doped Cz–Si may suffer from bulk degradation possibly attributed to boron–oxygen light induced degradation even if passivated by a tunneling oxide underlying n-doped poly-Si layers [7]. In addition, a significant lowering of effective excess carrier lifetime τ_{eff} on such TOPCon structures has been reported to occur due to surface-related degradation [8,9]. Another source of degradation is the occurrence of light- and elevated temperature-induced degradation (LeTID). Although in principle it is possible to suppress LeTID to a minimum by suitable high-temperature processing (e.g., lowering H content in the bulk [10,11]), the extent in varying sample structures regarding long-term stability is still open for research.

In this work, the influence of varying peak firing temperature on the hydrogen concentration in the crystalline silicon (c-Si) bulk is investigated for Ga-doped Cz–Si (Cz–Si:Ga) with symmetrically deposited P-doped polycrystalline silicon ((n)poly-Si). Hereby, the formation of defects during long-term stability testing is correlated with the observed H contents. In addition, various sample structures involving symmetrical and asymmetrical structures are investigated concerning their degradation behavior.

* Corresponding author.
E-mail address: joshua.kamphues@uni-konstanz.de (J. Kamphues).

https://doi.org/10.1016/j.solmat.2024.113156
Received 30 July 2024; Received in revised form 2 September 2024; Accepted 3 September 2024
Available online 7 September 2024
0927-0248/© 2024 The Author(s). Published by Elsevier B.V. This is an open access article under the CC BY license (http://creativecommons.org/licenses/by/4.0/).

Konstanzer Online-Publikations-System (KOPS)
URL: http://nbn-resolving.de/urn:nbn:de:bsz:352-2-17o2sq56s1gp65

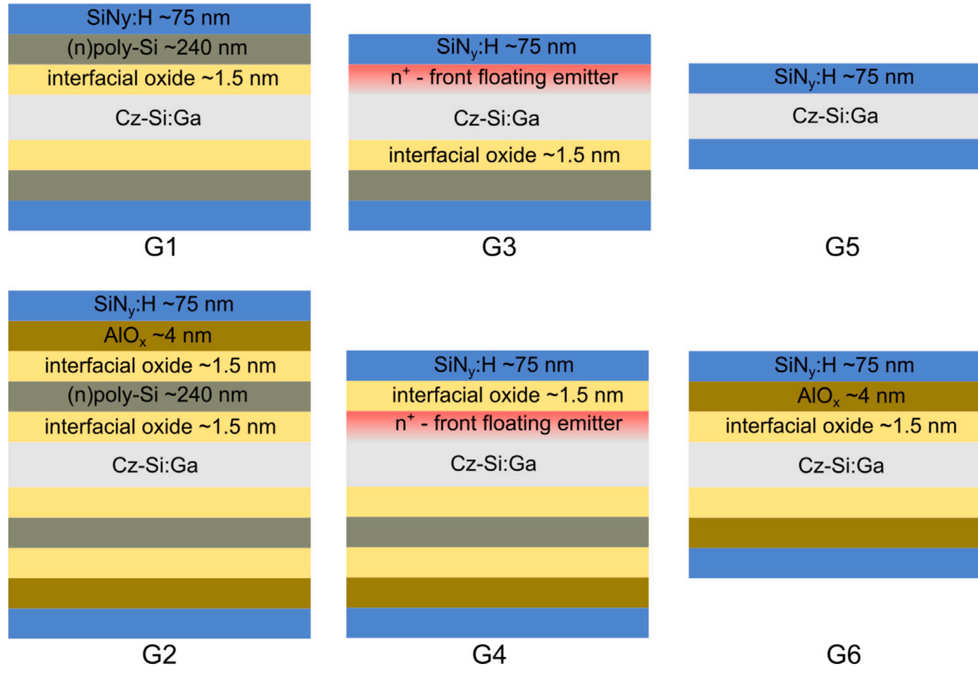

Fig. 1. Sample overview that was used for investigations. G1 was processed with an (n)a-Si layer on both sides, while G3 solely received a single-sided (n)a-Si layer. Due to the crystallization of the (n)a-Si during a $POCl_3$ diffusion, G3 has an additional front floating emitter. G5 serves as a reference without any poly-Si. G2, G4 and G6 only differ from G1, G3 and G5 by an additional interfacial oxide and an AlO_x layer below the SiN_y:H.

2. Methodology

2.1. Material and preprocessing

For this study, Cz–Si:Ga (1.6 Ω cm) wafers of M2 size were saw-damage etched in KOH, followed by wet chemical cleaning procedures, resulting in a final wafer thickness of ∼150 μm. Depending on the sample structures a thermal tunnel oxide was grown subsequently, followed by the deposition of a ∼240 nm thick P-doped amorphous silicon ((n)a-Si:H) by plasma-enhanced chemical vapor deposition (PECVD), either on both sides or just one side of the wafer. Afterwards, the (n)a-Si:H was crystallized during a $POCl_3$ diffusion. Both, $POCl_3$ diffusion and forming of the TOPCon structure are known as effective gettering steps. On a planar c-Si surface, this diffusion yields a sheet resistance of ∼320 Ω sq^{-1}, the doping level of the (n)poly-Si layer is only marginally affected. After the removal of the phosphorus silicate glass layer, an optimized SiN_y:H passivation and anti-reflective layer were deposited using PECVD. Additionally, for some samples, a thin PECVD AlO_x layer was deposited after growing a thermal oxide and before depositing the SiN_y:H layer on top. The four resulting sample groups, as well as two reference groups without any (n)a-Si:H deposition or $POCl_3$ diffusion, are illustrated in Fig. 1. All wafers were fired in an industrial belt furnace at a measured sample peak temperature of 800 °C, monitored using a k-type thermocouple placed at the center of the sample. For the variation of peak firing furnace temperature, samples from G2 did not receive a $POCl_3$ diffusion for crystallization but were instead crystallized in an annealing step carried out at the same temperature as the diffusion. The samples were then fired at four measured sample temperatures of T_1 = 700 °C, T_2 = 750 °C, T_3 = 800 °C and T_4 = 850 °C. Four 5 cm × 5 cm samples were cut from each wafer before further treatment.

2.2. Accelerated long-term stability treatment and characterization

The injection-dependent effective excess carrier lifetime $\tau_{\mathrm{eff}}(\Delta n)$ measurements were done using photoconductance decay (PCD) [12, 13] at 30 °C using a WCT-120 device from Sinton Instruments. Accelerated long-term stability experiments were carried out on a hot-plate at 130(1) °C with illumination being photon-flux equivalent to 1.0(1) sun [14], using halogen lamps. The illuminated annealing was interrupted from time to time for PCD measurements to monitor changes in τ_{eff}. Occurring changes in lifetime are evaluated by the calculation of a lifetime equivalent defect density

$$\Delta N_{\mathrm{leq}} = \frac{1}{\tau_{\mathrm{eff}}(t)} - \frac{1}{\tau_{\mathrm{eff}}(0)} \tag{1}$$

which serves as a good measure for the formation and dissociation of defects without knowledge of absolute defect levels [15]. The term $\Delta N_{\mathrm{leq,max}}$ refers to the maximum extent of ΔN_{leq} of an individual sample that appears during treatment. All evaluated effective lifetimes and defect densities were assessed at an injection level $\Delta n = 5 \cdot 10^{15}$ cm^{-3} if not stated otherwise. The reason for this specific injection is edge-related recombination as discussed in Appendix A.1.

Further analysis is carried out for the long-term stability treatment of symmetrical and asymmetrical TOPCon samples in comparison to reference samples without (n)poly-Si. Hereby, a deep-level defect species is assumed. The injection-dependent dataset of ΔN_{leq} is evaluated regarding maximum bulk related ($\Delta n \rightarrow 0$) lifetime equivalent defect densities $\Delta N^{*}_{\mathrm{leq}}$ and surface related saturation current density ΔJ_0 [16]. Initial surface-related J_0 is evaluated by the slope-based approach [17] using the parametrization from Niewelt et al. [18] for an intrinsic lifetime with maximal photon recycling. For all samples, J_0 is given as a mean for both sample sides.

2.3. Assessment of bulk hydrogen concentration

The formation of overall neutral gallium-hydrogen pairs from hydrogen dimers may be exploited for the quantification of hydrogen concentration in the bulk [19]. In particular, the splitting of neutral dimers H_2 to H^+ as intermediate species consumes holes h^+ and results in a measurable change in hole concentration p_0 during dark annealing according to the reaction [20,21]

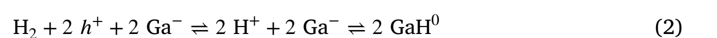

$$H_2 + 2\,h^+ + 2\,Ga^- \rightleftharpoons 2\,H^+ + 2\,Ga^- \rightleftharpoons 2\,GaH^0 \tag{2}$$

After GaH pair formation is largely completed, subsequent illuminated annealing can be used to dissociate nearly all GaH pairs [22]. GaH pair formation in this work was induced during dark annealing at 180(1) °C with interruptions to measure the change in hole concentration by resistivity measurements. For the dissociation of GaH pairs an illumination at 300(2) °C and a photon-flux equivalent of 2.0(2) suns was used.

The initial species concentrations of GaH pairs $[GaH]_{init}$ and hydrogen dimers $[H_2]_{init}$ can be concluded from the initial hole concentration $p_{0,init}$, that after dark annealing $p_{0,da}$ and after illuminated annealing $p_{0,il}$ by

$$[GaH]_{init} = p_{0,il} - p_{0,init} \tag{3}$$

$$[H_2]_{init} = \frac{1}{2}\left(p_{0,init} - p_{0,da}\right) \tag{4}$$

From this the total hydrogen concentration follows according to

$$[H] = 2\,[H_2]_{init} + [GaH]_{init} \tag{5}$$

The factor $\frac{1}{2}$ in Eq. (4) considers the formation of two GaH pairs from one H_2 dimer. Naturally, this is only valid for the assumptions that the majority of H_2 is involved in the GaH pairs formation and that almost all pairs can be dissociated during illuminated anneal.

The correlation between $[H_2]_{init}$ and the observed extent of degradation is suggested by several studies that varied the hydrogen concentration by different means, resulting in increased defect formation when more hydrogen is present [11,23–26]. In this study, the maximum extent of lifetime equivalent defect density ($\Delta N_{leq,max}$) or maximal bulk-related lifetime equivalent defect density ($\Delta N^{*}_{leq,max}$) is used to correlate the amount of defects formed with the hydrogen concentration present in the bulk.

In our case, hydrogen was introduced into the bulk by diffusion from a SiN_y:H layer during firing. For hydrogen quantification, samples were prepared similarly to [19] where electrical contacts were established using two pairs of Al pads on opposing sides on the back side of the substrate, deposited via electron-beam vapor deposition. Laser-fired contacts [27] provided electrical contact to the substrate for samples without additional (n)poly-Si or n^+ front floating emitter. For samples with (n)poly-Si on the back-side of the sample the aforementioned preparation would yield the resistance of the (n)poly-Si layer and not the bulk, hence, SiN_y:H was locally ablated by a 355 nm picosecond pulsed laser [28]. Afterwards, the (n)poly-Si was locally etched back in KOH and contacts with the Cz–Si:Ga were established via laser firing of evaporated Al as described before. This whole process is schematically shown in Fig. 2. All measurements were conducted on a temperature-stabilized 4-terminal setup at room temperature [19] and change in hole concentration p_0 was calculated using hole mobility data obtained from PV Lighthouse [29].

3. Results and discussion

3.1. Impact of peak firing temperature on the (n)poly-Si

3.1.1. Initial characterization after firing

Parameters τ_{eff}, J_0 and implied open-circuit voltage iV_{OC} are investigated for (n)poly-Si samples that are symmetrically capped with $SiO_z/AlO_x/SiN_y$:H (G2) and fired in a belt furnace at measured peak sample temperatures between 700 °C to 850 °C. For each peak temperature, at least two wafers were measured at nine positions. The corresponding results from PCD measurements are shown in Fig. 3. The excess carrier lifetime (at $\Delta n = 5 \cdot 10^{15}$ cm^{-3}) remains relatively constant at 2.5 ms up to a firing temperature of 800 °C, where a drop of ~400 µs occurs. Surface related J_0 remains at ~2 f A cm^{-2}, but variation across the wafer is increased for 800 °C. Implied open-circuit voltage is slightly reduced from ~743 mV to ~741 mV at 800 °C. For samples that were fired at 850 °C, the overall sample homogeneity and performance are significantly reduced which has been reported before for (n)poly-Si on B-doped material [30]. The variation of peak firing temperature in this work is additionally carried out on samples where a stack of SiO_z/SiN_y caps the (n)poly-Si without an additional AlO_x interlayer (G1). Since these results show very similar results but are lacking statistics, they are not shown here.

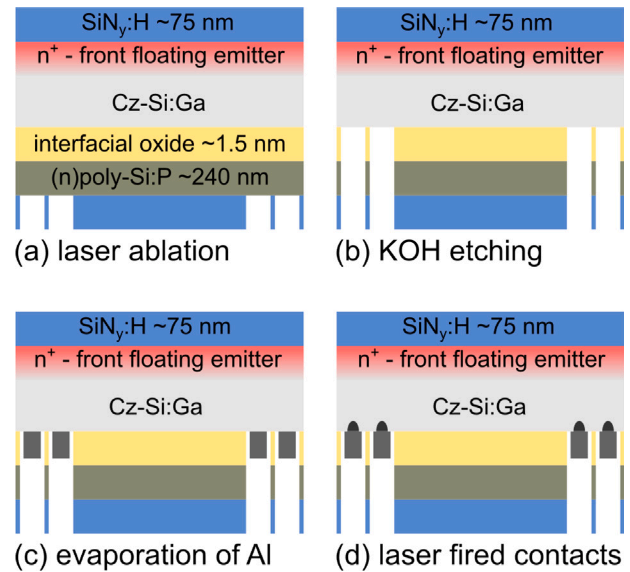

Fig. 2. Process to establish contacts with the Cz–Si:Ga underneath the TOPCon layers, exemplarily shown for G3. The process consists of (a) laser ablation, (b) etching in KOH, (c) evaporation of Al and (d) establishing contacts by laser firing.

The drastic deterioration for samples fired at 850 °C can be explained by visible blistering of the samples especially towards the edges of the samples. This is most likely related to an excess of hydrogen at the (n)poly-Si/c-Si interface which may lead to a delamination of the (n)poly-Si [31]. Therefore, samples should not be fired at a measured peak sample temperature way above 800 °C.

3.1.2. Long term stability-behavior

The investigation of long-term stability behavior for samples from G1 and G2 is performed for peak firing temperatures of 700 °C (T_1), 750 °C T_2 and 800 °C T_3 since a manageable homogeneity of samples fired at 850 °C is not given. Fig. 4 depicts τ_{eff}, ΔN_{leq} and J_0 evaluated from the long-term stability treatment at an illumination of 1.0(1) sun at 130 °C of samples G1 and G2. Effective lifetime measurements show that the initial lifetime is lowest for T_3 as already observed in Fig. 3. After ~0.2 h of treatment a minimum in lifetime for both sample types fired at 800 °C can be observed, which is visible as a maximum in ΔN_{leq}. For the peak temperature T_2 the degradation extent is significantly reduced and for T_1 barely any defects are formed or dissolved during the first hour of the treatment. After ~4 h of illuminated anneal, ΔN_{leq} is rising for all samples which can be explained by an increase of J_0, shown in the bottom graph of Fig. 4. The degradation and regeneration (especially for T_2 and T_3) during the first few hours of treatment can be attributed to the bulk as J_0 is barely affected. The course of the effective lifetime during such degradation is usually followed by regeneration, which is commonly observed, especially for LeTID in p-type Si [32]. Note that both, degradation and regeneration rates depend on treatment conditions, e.g. injection and sample temperature. In Fig. 4 the regeneration is only observable after defects have formed in the case of higher firing temperatures. Another experiment conducted at 180 °C show, that differences in SRD between G1 and G2 are marginal for the different firing temperatures (see Appendix A.2).

Overall ΔN_{leq} remains comparatively low during the treatment, indicating a reduced susceptibility to LeTID. This is discussed in more detail in Section 3.2.

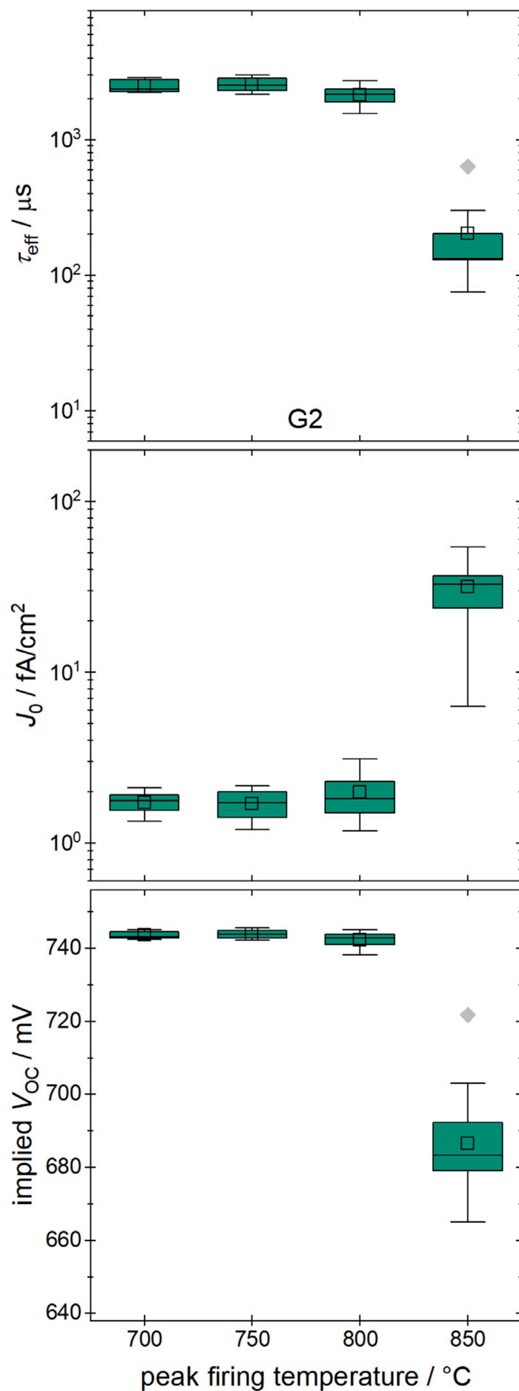

Fig. 3. Effective excess carrier lifetime τ_{eff}, surface related saturation current density J_0, and implied open-circuit voltage iV_{OC} after firing at different measured peak samples temperatures for symmetrical $SiO_z/AlO_x/SiN_y$ capped (n)poly-Si samples on Cz–Si:Ga.

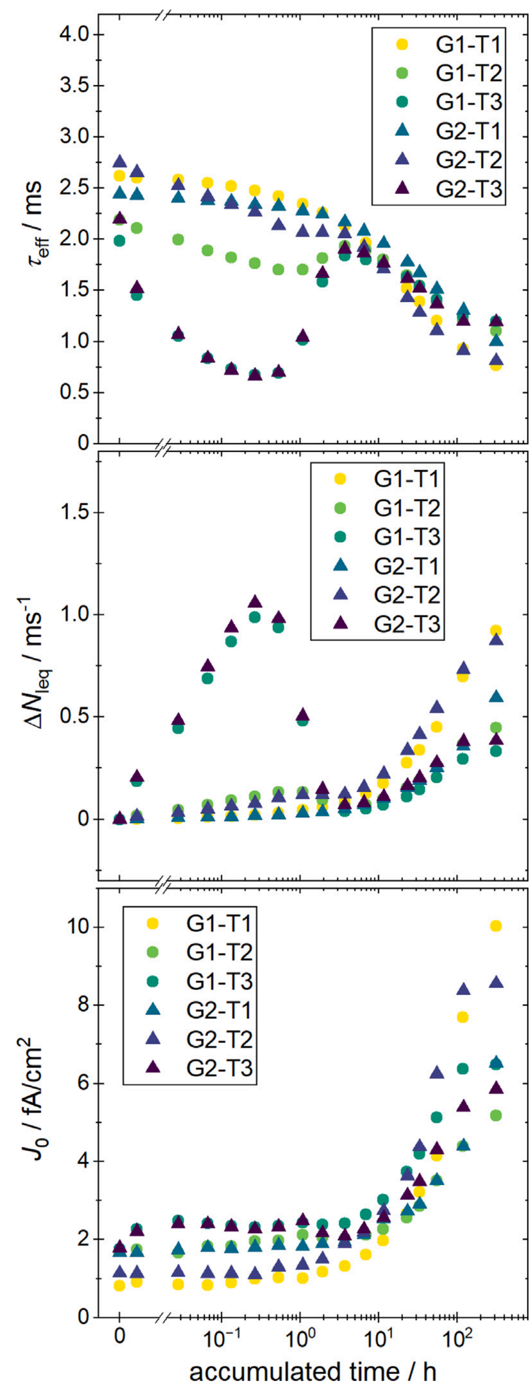

Fig. 4. τ_{eff}, ΔN_{leq} evaluated at $\Delta n = 5 \cdot 10^{15}$ cm^{-3} and surface related J_0 for G1 and G2 fired at T_1 = 700 °C, T_2 = 750 °C and T_3 = 800 °C during treatment under 1.0(1) sun illumination on a hotplate at 130(1) °C.

3.1.3. Correlation with the hydrogen content

From literature it is suggested that the peak firing temperature changes the amount of hydrogen present in the bulk, or more precisely, an increased peak temperature may lead to higher H concentrations in the c-Si [26,33]. By the change of peak temperature the cooling rate is changed as well, which also influences the effusion of H during the cooling phase. Therefore, resistivity samples were processed according to Fig. 2 for G1 and G2 with a variation of peak firing temperatures T_1, T_2 and T_3 to investigate the influence of (n)poly-Si on the bulk hydrogen concentration. In Fig. 5 the initial concentrations $[H_2]_{init}$ and $[GaH]_{init}$ as well as the total hydrogen concentration are shown over the observed $\Delta N_{leq,max}$. The latter increases for both sample types with rising peak fire temperature up to $2.5 \cdot 10^{15}$ cm^{-3}. A similar trend is observed for the initial species concentrations $[H_2]_{init}$ and $[GaH]_{init}$.

For the samples fired at T_1, hardly any $[H_2]_{init}$ was found. Interestingly, these are also the samples where hardly any degradation in the c-Si bulk occurs. This matches the hypothesis that hydrogen dimers, not GaH pairs, are the main source of hydrogen responsible for LeTID [26].

There is barely any difference in the initial dimer concentration between the sample groups G1 and G2. Since the difference is very low, it is possible that the AlO_x does not have a significant influence on the

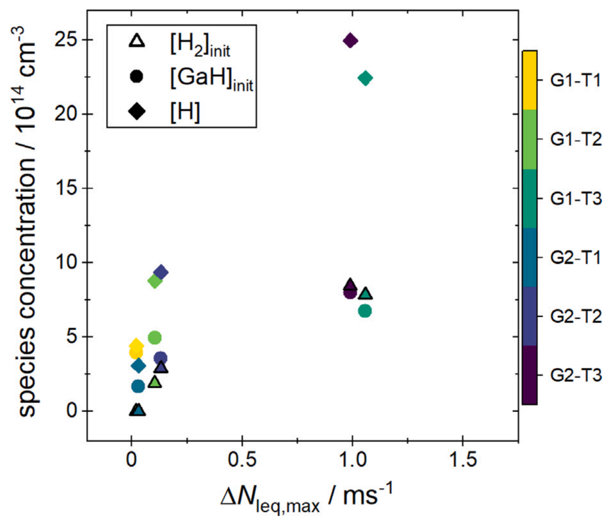

Fig. 5. Species concentration of $[H_2]_{init}$, $[GaH]_{init}$ and [H] correlated with the maximum lifetime equivalent defect density for samples passivated with poly-Si and two different passivation stacks for three different measured peak firing temperatures of T_1 = 700 °C, T_2 = 750 °C and T_3 = 800 °C.

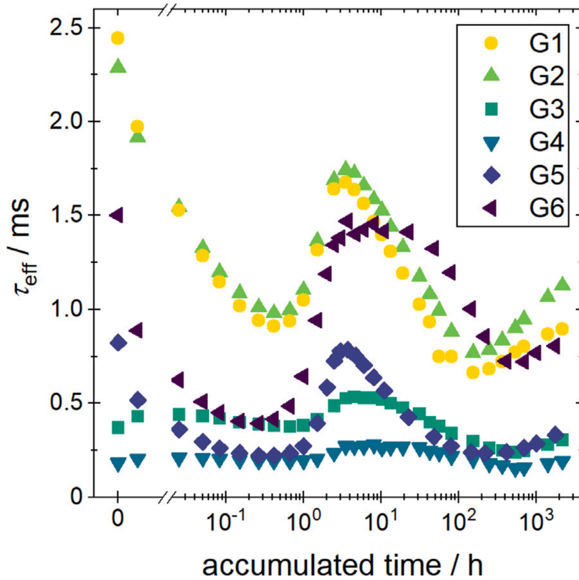

Fig. 6. Change in excess carrier lifetime τ_{eff} at $\Delta n = 5 \cdot 10^{15}$ cm^{-3} during treatment with 1.0(1) sun at a temperature of 130(1) °C for samples structures from G1 to G6.

hydrogen concentration in the bulk. Overall it seems, that samples with a symmetrical (n)poly-Si show a reduced remaining total hydrogen or at least $[H_2]_{init}$ for lower peak firing temperatures as it was observed before the samples without TOPCon-like structures [26,33]. Here, the amount of $[H_2]_{init}$ compared to references without TOPCon structures will be discussed for a peak temperature of 800 °C (see Section 3.2.2).

3.2. Variation of sample structure

3.2.1. Long-term stability behavior

Since symmetrical (n)poly-Si samples are not very applicable for solar cell concepts, a comparison is made with possible precursor structures that may be used similarly for IBC solar cells. Therefore, the different sample structures shown in Fig. 1, involving samples with at least one side of (n)poly-Si for G1 to G4 and reference samples only capped with SiN_y (G5) or $SiO_z/AlO_x/SiN_y$ (G6), are treated at an elevated temperature of 130(1) °C under illumination of 1 sun. The results for τ_{eff} for these samples are depicted in Fig. 6. The initial excess carrier lifetime for the symmetrical groups G1 and G2 is similar to that of samples shown in Fig. 4. Blistering occurring on asymmetrical samples with (n)poly-Si on the backside and a front floating emitter on the front (G3 and G4) during firing may be the reason for reduced lifetimes. For the reference samples, an additional SiO_z/AlO_x capping improved the initial lifetime compared to passivation with SiN_y:H only.

A more detailed analysis on the long-term stability is given in Fig. 7 by ΔN_{leq}, ΔN^*_{leq} and J_0 over the treatment time under an illumination being photon-flux equivalent to 1.0(1) sun at 130(1) °C. The observed maximum lifetime equivalent defect density in the top graph seems to be lowest for the first three groups G1 to G3 at ~0.8 ms^{-1} and is increased for the other groups with the reference that is only capped by SiN_y showing the highest degradation extent. However, J_0 is improving for some groups during the first ~4 h of the treatment, in particular G3 and G4, which lowers the observed ΔN_{leq} during this phase. Evaluating ΔN^*_{leq} offers the possibility to separate this surface-related improvement from the observed change in bulk-related defect densities.

In the middle graph of Fig. 7 the defect density ΔN^*_{leq} is lowest for the symmetrical (n)poly-Si samples but is increased for the asymmetrical stacks and still the highest for the references. Except for the symmetrical (n)poly-Si samples, ΔN^*_{leq} is lower for samples with additional SiO_z/AlO_x stacks compared to the single SiN_y passivation.

Surface-related degradation can be observed after ~4 h of treatment and is highest for the samples that have at least one side of SiN_y:H passivation without additional stacks. For G1 and G2 a reduced SRD can be seen. The lowest observed SRD is present for the reference sample G6.

3.2.2. Correlation with the hydrogen content

The hydrogen content in the different sample structures is again accessed as described in Section 2.3. The species concentrations of $[H_2]_{init}$, $[GaH]_{init}$ and [H] for all six groups in correlation with the evaluated maximal bulk-related lifetime equivalent defect density are shown in Fig. 8. In this case ΔN^*_{leq} is used because of the influence of surface-related improvement of samples G3 and G4 during the first few hours of treatment.

Total hydrogen concentration [H] and $[H_2]_{init}$ is highest for the SiN_y:H reference G5, which also shows the highest degradation extent. For the AlO_x reference G6 degradation extent and hydrogen content is already reduced. This can be explained by earlier studies regarding the role of AlO_x as a hydrogen diffusion barrier [11,34,35] during firing. As already mentioned in the previous section, this effect is not visible by the comparison between the symmetrical (n)poly-Si samples G1 and G2. It is therefore reasonable that the AlO_x only acts as a hydrogen diffusion barrier when there is no (n)poly-Si underneath. Overall the (n)poly-Si seems to have more advantageous properties regarding hydrogen content in the c-Si as bulk-related degradation is significantly reduced. The usage of a one-sided (n)poly-Si already lowers the hydrogen content and therefore degradation extent. An explanation might be that the poly-Si is acting as a H sink, leaving less hydrogen in the c-Si that could be harmful due to the involvement in the formation of the LeTID defect and subsequent SRD. Interestingly, the concentration of initially present GaH pairs is highest for the samples G1 and G2 but is rather relatively constant for all sample variations. An interpretation could be that the (n)poly-Si supports an increase of initially present GaH pairs.

Comparing the results for the symmetrical (n)poly-Si samples with the results of samples fired at 800 °C in Fig. 5, the total hydrogen concentration is very similar around ~$2.5 \cdot 10^{15}$ cm^{-3}. However, $[H_2]_{init}$ is lower and $[GaH]_{init}$ is higher in this section. This seems reasonable when comparing the maximum degradation extent in the top graph of Fig. 7 with Fig. 5 to compare ΔN_{leq} at the same injection level, as ΔN_{leq} is higher for the experiment with peak firing temperature variation, which might be induced by a changed cooling rate during firing.

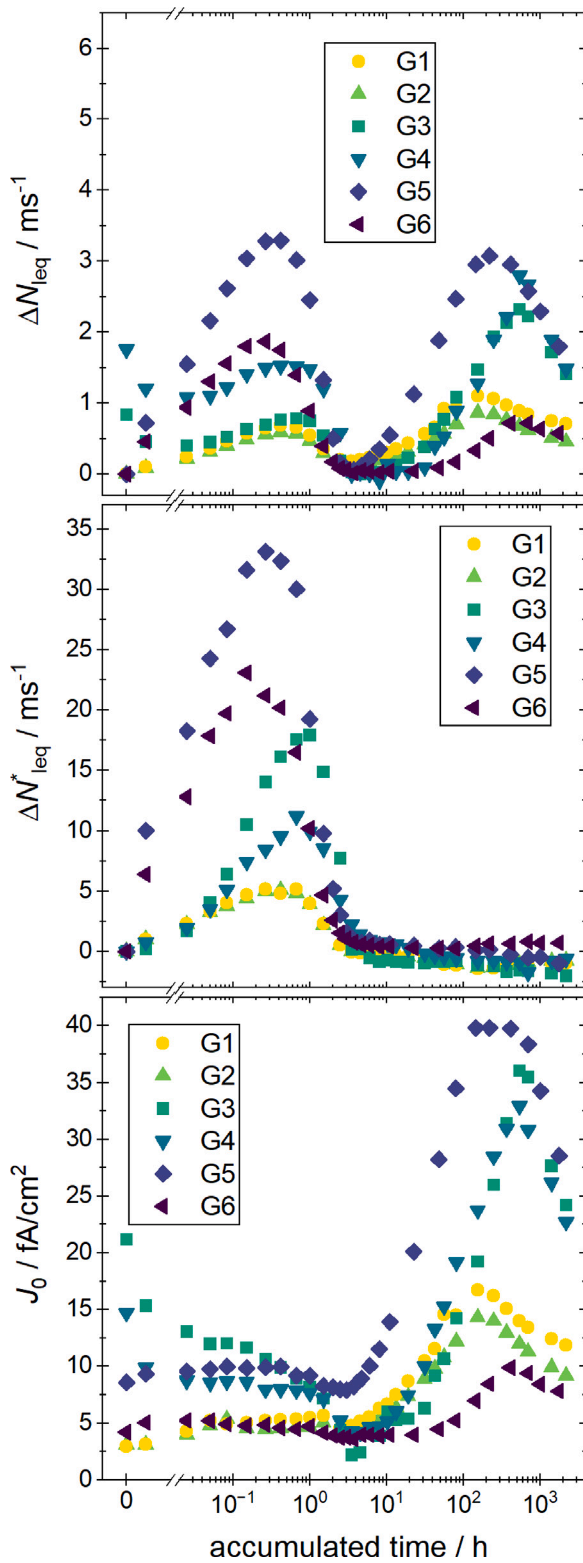

Fig. 7. Results of the long-term stability treatment for ΔN_{leq}, ΔN^*_{leq} and surface related J_0 for all samples G1 to G6 under an illumination of 1.0(1) sun at 130(1) °C.

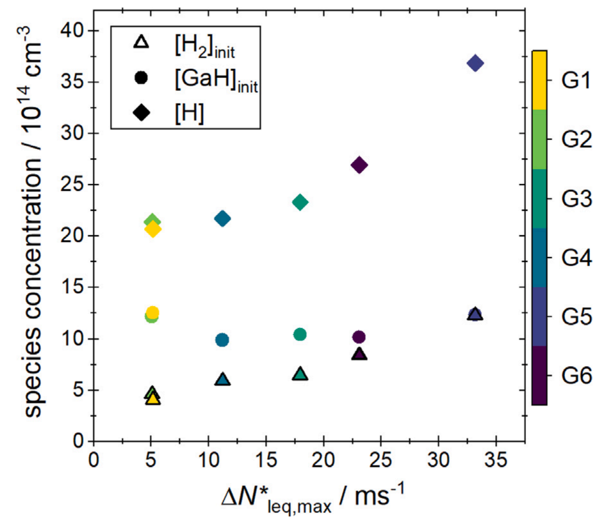

Fig. 8. Correlation between $\Delta N_{leq,max}$ and the concentrations of $[H_2]_{init}$, $[GaH]_{init}$ and [H] for the different sample structures G1 to G6.

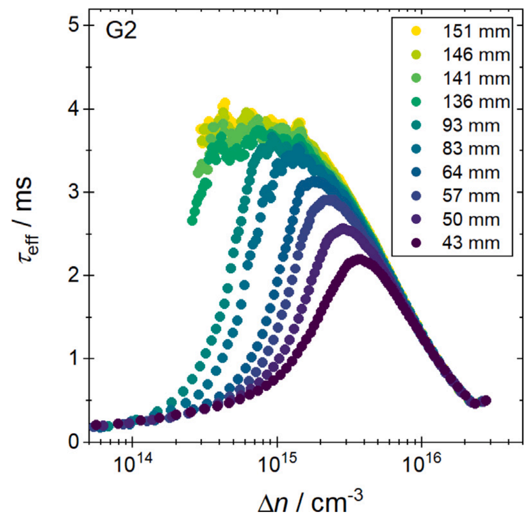

Fig. 9. Injection dependent measurement of τ_{eff} for a sample from G2 which is cut down from a side length of 151 mm to 43 mm The absolute measuring position remained the same as the same amount of material is taken away from all sides of the wafer.

4. Conclusion

In this study the influence of varying peak firing temperature between 700 °C and 850 °C on samples with passivating contacts, using (n)poly-Si on Cz–Si:Ga capped by $SiO_z/AlO_x/SiN_y$ or just SiN_y were investigated. A clear drop in performance at measured peak temperatures well above 800 °C was found related to the onset of blistering. Stability experiments at elevated temperatures and under illumination showed that significant degradation can only be observed for firing temperatures well above 750 °C. Yet, SRD might be increased for lower firing temperatures. The increased $\Delta N_{leq,max}$ was correlated with an increase in the initially present concentration of H_2 dimers. However, no difference between the usage of a different capping layer on the (n)poly-Si could be observed. This suggests that the role of a thin AlO_x is comparatively insignificant when using the (n)poly-Si, which might act as an effective sink for H alone.

By comparison of asymmetrical TOPCon sample structures in a long-term stability experiment, it was found that the degradation extent for samples with an SiO_z/AlO_x capping is reduced compared to only using SiN_y except for samples with symmetrical (n)poly-Si. Furthermore, the degradation extent is generally lower for samples that received an (n)poly-Si layer at least on one side of the sample. Resistivity measurements revealed that the $[H_2]_{init}$ concentration is the lowest for symmetrical (n)poly-Si out of all samples investigated resulting in the lowest observed degradation extent. TOPCon structures used in this

work are therefore, under comparable firing conditions, less susceptible to LeTID.

CRediT authorship contribution statement

Joshua Kamphues: Writing – original draft, Investigation, Validation, Formal analysis, Visualisation, Data curation, Conceptualization. **Jessica Lison:** Investigation. **Jana-Isabelle Polzin:** Writing – review & editing, Investigation. **Andreas Wolf:** Resources. **Jan Lossen:** Resources. **Axel Herguth:** Writing – review & editing. **Giso Hahn:** Writing – review & editing, Resources. **Fabian Geml:** Supervision, Conceptualization.

Declaration of competing interest

The authors declare that they have no known competing financial interests or personal relationships that could have appeared to influence the work reported in this paper.

Data availability

Data will be made available on request.

Acknowledgments

The authors would like to thank Benjamin Gapp for helpful discussions regarding laser ablation and Bärbel Rettenmaier for technical support. Part of this work was funded by the German Federal Ministry of Economic Affairs and Climate Action (BMWK) under contract numbers 03EE1102C and 03EE1148D. The content is the responsibility of the authors.

Appendix. Supplementary information

A.1. Edge-related recombination

It was found that some of the investigated sample structures, in particular those that feature a layer that collects excess carriers like (n)poly-Si on a p-type substrate, may suffer from long-range edge-related recombination which was already observed by others [36,37]. Fig. 9 shows the injection-dependent τ_{eff} of a G2 sample (see Fig. 1) for different sizes. Hereby, the wafer is cut down at all sides and measured at the center. The injection dependence of carrier lifetime seems unaffected as long as the wafer is completely intact and the edges are far away from the measuring spot. However, the smaller the sample gets, the more τ_{eff} is massively reduced towards lower injections. A similar experiment with photoluminescence imaging was carried out for varying distances in a recent study [38]. Since all long-term stability measurements are carried out with samples that have an edge length of 50 mm, most of the evaluation of carrier lifetimes is performed at $\Delta n = 5 \cdot 10^{15}$ cm^{-3} as for this injection, the measurement does not seem to be significantly influenced by that long-range edge-related recombination. However, one should note that the injection dependence of ΔN_{leq} for a deep-level defect, in particular with a high τ_n/τ_p ratio which is around 30 for LeTID [39,40], implies increasing ΔN_{leq} values when evaluated at lower injection levels [15]. Hence, comparisons with ΔN_{leq} data evaluated at different injection Δn or $\Delta n/p_0$ ratio should be taken with care.

A.2. J_0 evolution of samples with variation in peak fire temperature

Fig. 10 shows the evolution of J_0 during additional accelerated long-term stability experiments for G1 and G2 that were fired at measured peak temperatures T_1, T_2 and T_3. The treatment is carried out under an illumination of 1.0(1) sun at 180(1) °C.

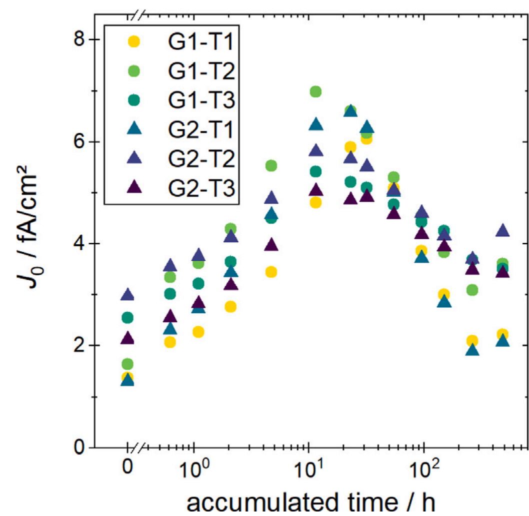

Fig. 10. Evolution of J_0 for samples of G1 and G2 during a treatment with an illumination of 1.0(1) sun on a hotplate at 180(1) °C. Both sample groups were fired at temperatures T_1, T_2 and T_3.

References

[1] D.K. Ghosh, S. Bose, G. Das, S. Acharyya, A. Nandi, S. Mukhopadhyay, A. Sengupta, Fundamentals, present status and future perspective of TOPCon solar cells: A comprehensive review, Surf. Interfaces 30 (2022) 101917, http://dx.doi.org/10.1016/j.surfin.2022.101917.

[2] A. Richter, J. Benick, F. Feldmann, A. Fell, M. Hermle, S.W. Glunz, n-type Si solar cells with passivating electron contact: Identifying sources for efficiency limitations by wafer thickness and resistivity variation, Sol. Energy Mater. Sol. Cells 173 (2017) 96–105, http://dx.doi.org/10.1016/j.solmat.2017.05.042.

[3] M. Fischer, International technology roadmap for photovoltaic (ITRPV), 2023, URL: www.itrpv.org.

[4] F. Haase, C. Hollemann, S. Schäfer, A. Merkle, M. Rienäcker, J. Krügener, R. Brendel, R. Peibst, Laser contact openings for local poly-si-metal contacts enabling 26.1%-efficient POLO-IBC solar cells, Sol. Energy Mater. Sol. Cells 186 (2018) 184–193, http://dx.doi.org/10.1016/j.solmat.2018.06.020.

[5] R. Kopecek, F. Buchholz, V.D. Mihailetchi, J. Libal, J. Lossen, N. Chen, H. Chu, C. Peter, T. Timofte, A. Halm, Y. Guo, X. Qu, X. Wu, J. Gao, P. Dong, Interdigitated back contact technology as final evolution for industrial crystalline single-junction silicon solar cell, Solar 3 (1) (2022) 1–14, http://dx.doi.org/10.3390/solar3010001.

[6] L. Rachdi, J. Lossen, D. Rudolph, Y.P. Sharma, L.J. Koduvelikulathu, J.-I. Polzin, S. Schmidt, T. Pernau, A. Wolf, Development and process optimization of a p-IBC solar cell with PECVD deposited passivated contacts, in: 40th European Photovoltaic Solar Energy Conf. and Exhibition, 2023, http://dx.doi.org/10.4229/EUPVSEC2023/1AO.5.6.

[7] M. Winter, S. Bordihn, R. Peibst, R. Brendel, J. Schmidt, Degradation and regeneration of n$^+$-doped poly-si surface passivation on p-type and n-type Cz–Si under illumination and dark annealing, IEEE J. Photovolt. 10 (2) (2020) 423–430, http://dx.doi.org/10.1109/JPHOTOV.2020.2964987.

[8] D. Chen, C. Madumelu, M. Kim, B.V. Stefani, A. Soeriyadi, D. Kang, H.C. Sio, X. Zhang, P. Zhu, B. Hallam, M. Wright, Investigating the degradation behaviours of n$^+$-doped poly-Si passivation layers: An outlook on long-term stability and accelerated recovery, Sol. Energy Mater. Sol. Cells 236 (2022) 111491, http://dx.doi.org/10.1016/j.solmat.2021.111491.

[9] D. Kang, H.C. Sio, D. Yan, W. Chen, J. Yang, J. Jin, X. Zhang, D. Macdonald, Long-term stability study of the passivation quality of polysilicon-based passivation layers for silicon solar cells, Sol. Energy Mater. Sol. Cells 215 (2020) 110691, http://dx.doi.org/10.1016/j.solmat.2020.110691.

[10] F. Maischner, S. Maus, J. Greulich, S. Lohmüller, E. Lohmüller, P. Saint-Cast, D. Ourinson, H. Vahlman, K. Hergert, S. Riepe, S. Glunz, S. Rein, LeTID mitigation via an adapted firing process in p-type PERC cells from SMART cast-monocrystalline, czochralski and high-performance multicrystalline silicon, Prog. Photovolt. Res. Appl. 30 (2) (2022) 123–131, http://dx.doi.org/10.1002/pip.3467.

[11] A. Schmid, C. Fischer, D. Skorka, A. Herguth, C. Winter, A. Zuschlag, G. Hahn, On the role of AlO_x thickness in AlO_x/SiN_y:H layer stacks regarding light- and elevated temperature-induced degradation and hydrogen diffusion in c-Si, IEEE J. Photovolt. 11 (4) (2021) 967–973, http://dx.doi.org/10.1109/JPHOTOV.2021.3075850.

[12] R.A. Sinton, A. Cuevas, Contactless determination of current–voltage characteristics and minority-carrier lifetimes in semiconductors from quasi-steady-state photoconductance data, Appl. Phys. Lett. 69 (17) (1996) 2510–2512, http://dx.doi.org/10.1063/1.117723.

[13] H. Nagel, C. Berge, A.G. Aberle, Generalized analysis of quasi-steady-state and quasi-transient measurements of carrier lifetimes in semiconductors, J. Appl. Phys. 86 (11) (1999) 6218–6221, http://dx.doi.org/10.1063/1.371633.

[14] A. Herguth, On the meaning(fullness) of the intensity unit 'suns' in light induced degradation experiments, Energy Procedia 124 (2017) 53–59, http://dx.doi.org/10.1016/j.egypro.2017.09.339.

[15] A. Herguth, On the lifetime-equivalent defect density: properties, application, and pitfalls, IEEE J. Photovolt. 9 (5) (2019) 1182–1194, http://dx.doi.org/10.1109/JPHOTOV.2019.2922470.

[16] A. Herguth, J. Kamphues, On the impact of bulk lifetime on the quantification of recombination at the surface of semiconductors, IEEE J. Photovolt. 13 (5) (2023) 672–681, http://dx.doi.org/10.1109/JPHOTOV.2023.3291453.

[17] A. Kimmerle, J. Greulich, A. Wolf, Carrier-diffusion corrected J_0-analysis of charge carrier lifetime measurements for increased consistency, Sol. Energy Mater. Sol. Cells 142 (2015) 116–122, http://dx.doi.org/10.1016/j.solmat.2015.06.043.

[18] T. Niewelt, B. Steinhauser, A. Richter, B. Veith-Wolf, A. Fell, B. Hammann, N.E. Grant, L. Black, J. Tan, A. Youssef, J.D. Murphy, J. Schmidt, M.C. Schubert, S.W. Glunz, Reassessment of the intrinsic bulk recombination in crystalline silicon, Sol. Energy Mater. Sol. Cells 235 (2022) 111467, http://dx.doi.org/10.1016/j.solmat.2021.111467.

[19] A. Herguth, C. Winter, Methodology and error analysis of direct resistance measurements used for the quantification of boron–hydrogen pairs in crystalline silicon, IEEE J. Photovolt. 11 (4) (2021) 1059–1068, http://dx.doi.org/10.1109/JPHOTOV.2021.3074463.

[20] T. Zundel, J. Weber, Dissociation kinetics of shallow-acceptor-hydrogen pairs in silicon, MRS Online Proc. Libr. (OPL) 163 (1989) 443, http://dx.doi.org/10.1557/PROC-163-443.

[21] Y. Acker, J. Simon, A. Herguth, Formation dynamics of BH and GaH-pairs in crystalline silicon during dark annealing, Phys. Status Solidi A 219 (17) (2022) 2200142, http://dx.doi.org/10.1002/pssa.202200142.

[22] J. Simon, A. Herguth, L. Kutschera, G. Hahn, The dissociation of gallium–hydrogen pairs in crystalline silicon during illuminated annealing, Phys. Status Solidi RRL 16 (12) (2022) 2200297, http://dx.doi.org/10.1002/pssr.202200297.

[23] U. Varshney, M. Abbott, A. Ciesla, D. Chen, S. Liu, C. Sen, M. Kim, S. Wenham, B. Hoex, C. Chan, Evaluating the impact of SiN_x thickness on lifetime degradation in silicon, IEEE J. Photovolt. 9 (3) (2019) 601–607, http://dx.doi.org/10.1109/JPHOTOV.2019.2896671.

[24] C. Vargas, K. Kim, G. Coletti, D. Payne, C. Chan, S. Wenham, Z. Hameiri, Carrier-induced degradation in multicrystalline silicon: dependence on the silicon nitride passivation layer and hydrogen released during firing, IEEE J. Photovolt. 8 (2) (2018) 413–420, http://dx.doi.org/10.1109/JPHOTOV.2017.2783851.

[25] B. Hammann, N. Aßmann, J. Schön, W. Kwapil, F. Schindler, S. Roder, E.V. Monakhov, M.C. Schubert, Understanding the impact of the cooling ramp of the fast-firing process on light- and elevated-temperature-induced degradation, Sol. Energy Mater. Sol. Cells 259 (2023) 112462, http://dx.doi.org/10.1016/j.solmat.2023.112462.

[26] R. Zerfaß, J. Simon, A. Herguth, G. Hahn, Impact of hydrogen in ga-doped silicon on maximum LeTID defect density, Solar RRL 7 (22) (2023) 2300501, http://dx.doi.org/10.1002/solr.202300501.

[27] E. Schneiderlöchner, R. Preu, R. Lüdemann, S.W. Glunz, Laser-fired rear contacts for crystalline silicon solar cells, Prog. Photovolt. Res. Appl. 10 (1) (2002) 29–34, http://dx.doi.org/10.1002/pip.422.

[28] G. Heinrich, M. Bähr, K. Stolberg, T. Wütherich, M. Leonhardt, A. Lawerenz, Investigation of ablation mechanisms for selective laser ablation of silicon nitride layers, Energy Procedia 8 (2011) 592–597, http://dx.doi.org/10.1016/j.egypro.2011.06.188.

[29] P. Lighthouse, Various calculators, 2023, Available online: https://www.pvlighthouse.com.au/. (Accessed July 2023).

[30] C. Madumelu, Y. Cai, C. Hollemann, R. Peibst, B. Hoex, B.J. Hallam, A.H. Soeriyadi, Assessing the stability of p^+ and n^+ polysilicon passivating contacts with various capping layers on p-type wafers, Sol. Energy Mater. Sol. Cells 253 (2023) 112245, http://dx.doi.org/10.1016/j.solmat.2023.112245.

[31] S. Choi, O. Kwon, K.H. Min, M.S. Jeong, K.T. Jeong, M.G. Kang, S. Park, K.K. Hong, H.-E. Song, K.-H. Kim, Formation and suppression of hydrogen blisters in tunnelling oxide passivating contact for crystalline silicon solar cells, Sci. Rep. 10 (9672) (2020) 1–14, http://dx.doi.org/10.1038/s41598-020-66801-4.

[32] F. Kersten, P. Engelhart, H.-C. Ploigt, A. Stekolnikov, T. Lindner, F. Stenzel, M. Bartzsch, A. Szpeth, K. Petter, J. Heitmann, J.W. Müller, Degradation of multicrystalline silicon solar cells and modules after illumination at elevated temperature, Sol. Energy Mater. Sol. Cells 142 (2015) 83–86, http://dx.doi.org/10.1016/j.solmat.2015.06.015.

[33] J. Simon, R. Fischer-Süßlin, R. Zerfaß, L. Kutschera, P. Dufke, A. Herguth, S. Roder, G. Hahn, Correlation study between LeTID defect density, hydrogen and firing profile in Ga-doped crystalline silicon, Sol. Energy Mater. Sol. Cells 260 (2023) 112456, http://dx.doi.org/10.1016/j.solmat.2023.112456.

[34] U. Varshney, B. Hallam, P. Hamer, A. Ciesla, D. Chen, S. Liu, C. Sen, A. Samadi, M. Abbott, C. Chan, B. Hoex, Controlling light- and elevated-temperature-induced degradation with thin film barrier layers, IEEE J. Photovolt. 10 (1) (2019) 19–27, http://dx.doi.org/10.1109/JPHOTOV.2019.2945199.

[35] J. Kamphues, A. Schmid, R. Fischer-Süßlin, G. Hahn, F. Geml, Influence of AlO_x interlayers on LeTID kinetics in Ga-doped Cz–Si, SiliconPV Conf. Proc. 1 (2023) http://dx.doi.org/10.52825/siliconpv.v1i.842.

[36] M. Kessler, T. Ohrdes, P.P. Altermatt, R. Brendel, The effect of sample edge recombination on the averaged injection-dependent carrier lifetime in silicon, J. Appl. Phys. 111 (5) (2012) http://dx.doi.org/10.1063/1.3691230.

[37] B. Veith, T. Ohrdes, F. Werner, R. Brendel, P.P. Altermatt, N.-P. Harder, J. Schmidt, Injection dependence of the effective lifetime of n-type si passivated by Al_2O_3: An edge effect? Sol. Energy Mater. Sol. Cells 120 (2014) 436–440, http://dx.doi.org/10.1016/j.solmat.2013.06.049.

[38] R. Basnet, D. Yan, P. Phang, T. Truong, D. Kang, H. Shen, D. Macdonald, Understanding the strong apparent injection dependence of carrier lifetimes in doped polycrystalline silicon passivated wafers, Solar RRL 8 (12) (2024) 2400087, http://dx.doi.org/10.1002/solr.202400087.

[39] A.E. Morishige, M.A. Jensen, D.B. Needleman, K. Nakayashiki, J. Hofstetter, T.-T.A. Li, T. Buonassisi, Lifetime spectroscopy investigation of light-induced degradation in p-type multicrystalline silicon PERC, IEEE J. Photovolt. 6 (6) (2016) 1466–1472, http://dx.doi.org/10.1109/JPHOTOV.2016.2606699.

[40] D. Lin, Z. Hu, L. Song, D. Yang, X. Yu, Investigation on the light and elevated temperature induced degradation of gallium-doped Cz–Si, Sol. Energy 225 (2021) 407–411, http://dx.doi.org/10.1016/j.solener.2021.07.023.